

THE PHYSICS OF MICROWAVE BACKGROUND ANISOTROPIES [†]

Wayne Hu,¹ Naoshi Sugiyama,² & Joseph Silk³

¹*Institute for Advanced Study
School of Natural Sciences
Princeton, NJ 08540*

²*Department of Physics
and Research Center for the Early Universe
The University of Tokyo, Tokyo 113, Japan*

³*Department of Astronomy and Physics
and Center for Particle Astrophysics*

Cosmic microwave background anisotropies provide a vast amount of cosmological information. Their full physical content and detailed structure can be understood in a simple and intuitive fashion through a systematic investigation of the individual mechanisms for anisotropy formation.

whu@sns.ias.edu

Additional material can be found at <http://www.sns.ias.edu/~whu/physics/physics.html>

[†] Review for Nature, revised November 26, 2024.

An extraordinary wealth of cosmological information lies in the cosmic microwave background (CMB) temperature anisotropy at degree and subdegree scales. Yet despite the flurry of reported measurements in the past several years,¹ systematic errors, extragalactic sources and galactic foregrounds have prevented definitive measurements at these scales. With adequate sky and frequency coverage, foreground contamination can be avoided or removed.^{2,3} Experiments presently in the planning stage are expected to overcome such difficulties within the next few years. It is therefore timely to review the physics of anisotropy formation in order to lay the basis for the science that may be extracted from these anticipated detections.

A definitive set of experiments must achieve good sensitivity at an angular resolution of at least 10 arcminutes. Large angle anisotropies, detected by the *COBE* satellite,⁴ probe the fluctuations laid down in the very early universe, possibly the result of quantum mechanical processes during an epoch of inflation. These primordial fluctuations grew by gravitational instability into the large scale structure of the universe today. To reveal more cosmological information, one has to probe the anisotropy of the CMB at smaller angular scales where causal interactions take place. A causally-connected region, or horizon volume, at last scattering subtends no more than a degree on the sky under most conditions.

Inside the horizon, acoustic,⁵ Doppler,⁶ gravitational redshift,⁷ and photon diffusion⁸ effects combine to form a seemingly complicated spectrum of primary anisotropies. Considering the component contributions individually reveals the underlying simplicity and sensitivity of the spectrum to a variety of cosmological parameters, including the baryon density, the dark matter density, the cosmological constant, the Hubble constant, and the curvature of the universe. Secondary effects generated at later times may provide important clues for the process of structure formation. Furthermore, these degree and subdegree scale anisotropies will enable one to attempt a reconstruction of the spectrum and evolution of density fluctuations on 100 Mpc scales which deep galaxy redshift surveys are beginning to probe.

In this review, we draw on classical Newtonian analogues to represent anisotropy formation.^{9,10} We refer the reader elsewhere for alternate descriptions, which differ in perspective not in physical content, and more complete historical developments of the subject.^{11,12,13}

Primary Anisotropies

Before redshift $z_* \simeq 10^3$, CMB photons are hot enough to ionize hydrogen. Compton scattering tightly couples the photons to the electrons which are in turn coupled to the baryons by electromagnetic interactions. The system can thus be dynamically described as a photon-baryon fluid. Photon pressure resists gravitational compression of the fluid and sets up acoustic oscillations. At z_* , neutral hydrogen forms and the photons last scatter. Regions of compression and rarefaction at this epoch represent hot and cold spots respectively. Photons also suffer gravitational redshifts from climbing out of the potentials on the last scattering surface. The resultant fluctuations appear to the observer today as anisotropies on the sky. We call these fluctuations *primary* anisotropies. Secondary anisotropies can also be generated between recombination and the present. We consider those contributions in the next section.

Normal Modes

Normal mode analysis breaks the system into independent oscillators. In flat space, this corresponds to a Fourier decomposition of the fluctuation into plane waves of comoving wavenumber k . An isotropic temperature perturbation $\Theta = \Delta T/T$ in mode k evolves almost as a simple harmonic oscillator before recombination,¹⁴ $m_{\text{eff}}\ddot{\Theta} + k^2 c^2 \Theta/3 \simeq m_{\text{eff}}g$. The overdots represent derivatives with respect to conformal time $\eta = \int(1+z)dt$ and the effective dimensionless mass of the oscillator is $m_{\text{eff}} = 1 + R$. Here $R = (\rho_b + p_b)/(\rho_\gamma + p_\gamma) \simeq 3\rho_b/4\rho_\gamma$ is the baryon-photon momentum density ratio. The oscillation frequency obeys the dispersion relation $\omega = kc/\sqrt{3m_{\text{eff}}} = kc_s$, where c_s is the sound speed. Gravity provides an effective acceleration of $g = -k^2 c^2 \Psi/3 - \ddot{\Phi}$, where Ψ is the Newtonian gravitational potential and $\Phi \simeq -\Psi$ is the curvature perturbation on spatial hypersurfaces. These are related to the density fluctuation via the Poisson equation and give rise to gravitational infall and time dilation as we shall see.

Acoustic Oscillations

Let us first consider the case of a *static* potential.¹⁵ Here, $g \simeq -k^2 c^2 \Psi/3$ and supplies the usual gravitational force that causes matter to fall into potential wells. Since big bang nucleosynthesis implies that the baryon density is low, as a first approximation, assume that the photons completely dominate the fluid, $R \ll 1$.

Gravitational infall compresses the fluid until resistance from photon pressure reverses the motion. To complete the description, we need to choose the initial conditions, assumed for now to be adiabatic (see Box 1): $\Theta(0) = -\frac{2}{3}\Psi$ and $\dot{\Theta}(0) = 0$. Since a constant gravitational force merely shifts the zero point of the oscillation to $\Theta = -\Psi$, the initial displacement of $\frac{1}{3}\Psi$ from the zero point enters into the oscillation as $\Theta + \Psi = \frac{1}{3}\Psi \cos(ks)$, where the *sound horizon* is $s = \int c_s d\eta$ (see Fig. 1a). At last scattering η_* , the photons decouple from the baryons and stream out of potential wells suffering gravitational redshifts equal to Ψ . We thus call $\Theta + \Psi$ the *effective* temperature fluctuation. Here the redshift exactly cancels the zero point displacement since gravitational infall and redshift have the same physical origin if the baryons are dynamically insignificant.

The phase of the oscillation is frozen in at last scattering. The critical wavenumber $k_A = \pi/s_*$ corresponds to the sound horizon at that time (see Fig. 1a). Longer wavelengths will not have evolved from the initial conditions and possess $\frac{1}{3}\Psi$ fluctuations after gravitational redshift. This combination of the intrinsic temperature fluctuation and the gravitational redshift is the well-known Sachs-Wolfe effect.⁷ Shorter wavelength fluctuations can be frozen at different phases of the $\cos(ks_*)$ oscillation. As a function of k , there will be a harmonic series of temperature *fluctuation* peaks with $k_m = mk_A = m\pi/s_*$ for the m th peak. Odd peaks thus represent the compression phase (temperature crests), whereas even peaks represent the rarefaction phase (temperature troughs), inside the potential wells. More exotic models might produce a phase shift $\cos(ks_* + \phi)$, but even so the spacing between the peaks remains $k_m - k_{m-1} = k_A$ (see Box 1). Thus the sound horizon at last scattering $s_*(\Omega_0 h^2, \Omega_B h^2)$ should be measurable from the CMB. Here the Hubble constant is $H_0 = 100h \text{ km s}^{-1} \text{ Mpc}^{-1}$ and Ω_0 and Ω_B are the present matter and baryon density in units of the critical density. The dependence on $\Omega_B h^2$ is weak if $R(z_*) \simeq 30\Omega_B h^2 \ll 1$.

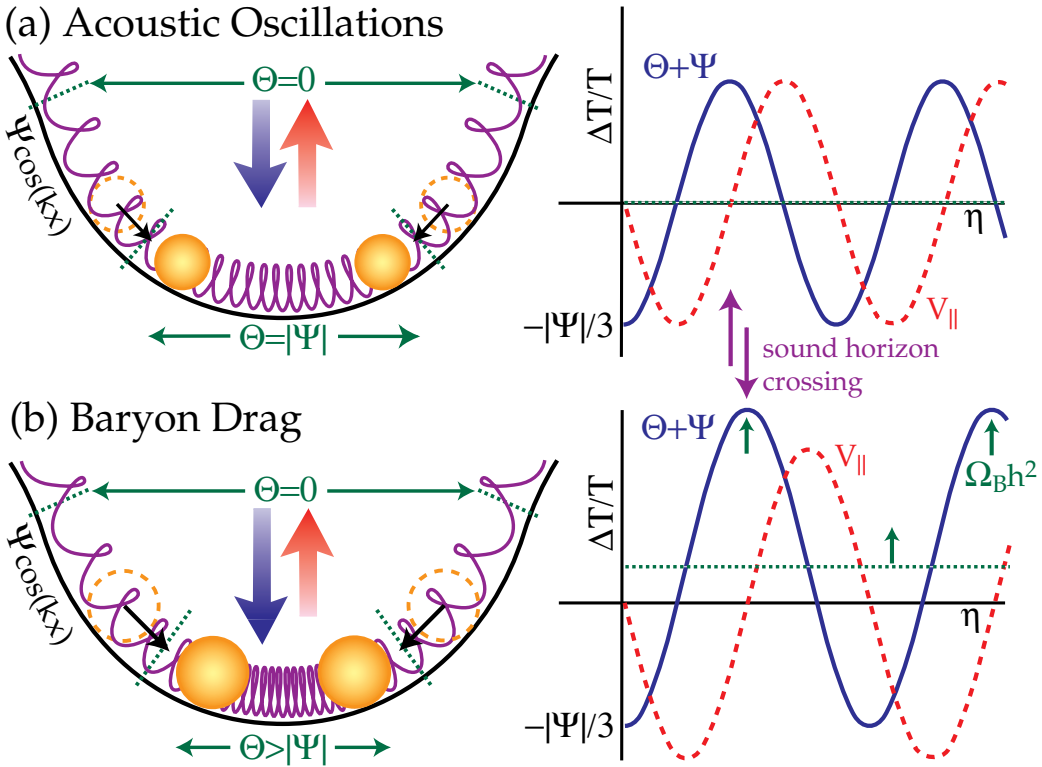


Figure 1. (a) Acoustic oscillations. Photon pressure resists gravitational compression of the fluid setting up acoustic oscillations (left panel, real space $-\pi/2 \lesssim kx \lesssim \pi/2$). Springs and balls schematically represent fluid pressure and effective mass respectively. Gravity displaces the zero point such that $\Theta \cos(kx) = -\Psi \cos(kx)$ at equilibrium with oscillations in time of amplitude $\Psi/3$ (right panel). The displacement is cancelled by the redshift $\Psi \cos(kx)$ a photon experiences climbing out of the well. Velocity oscillations lead to a Doppler effect V_{\parallel} shifted by $\pi/2$ in phase from the temperature perturbation. (b) Baryon drag increases the gravitating mass, causing more infall and a net zero point displacement, even after redshift. Temperature crests (compression) are enhanced over troughs (rarefaction) and Doppler contributions.

Baryon Drag

While effectively pressureless, the baryons do contribute to the mass of the fluid $m_{\text{eff}} = 1 + R$, where recall $R \propto \Omega_B h^2$. This changes the balance between pressure and gravity. In the presence of baryons, gravitational infall leads to greater compression of the fluid in a potential well, *i.e.* a further displacement of the oscillation zero point¹⁴ (see Fig. 1b). Since the redshift is not affected by the baryon content, this relative shift remains after last scattering to enhance all peaks from compression over those from rarefaction. If R were constant, $\Theta + \Psi = \frac{1}{3}\Psi(1+3R) \cos(ks) - R\Psi$, with compressional peaks a factor of $(1+6R)$ larger than the Sachs-Wolfe plateau and a difference in peak amplitude of $2R\Psi$ between even and odd peaks.⁵² In reality, these effects are reduced since $R \rightarrow 0$ at early times. Nevertheless, the relative peak heights probe $\Omega_B h^2$ through R and the amplitude of potential perturbations at last scattering through Ψ .

Finally the *evolution* of the effective mass influences the oscillation. In classical mechanics, the ratio of energy $\frac{1}{2}m_{\text{eff}}\omega^2 A^2$ to frequency ω of an oscillator is an adiabatic invariant. Thus for the slow changes in

$m_{\text{eff}} \propto \omega^{-2}$, the amplitude of the oscillation varies as $A \propto m_{\text{eff}}^{-1/4} \propto (1 + R)^{-1/4}$ representing a small decay with time.

Doppler Effect

Since the turning points are at the extrema, the fluid velocity oscillates $\pi/2$ out of phase with the density (see Fig. 1a). Its line-of-sight motion relative to the observer causes a Doppler shift. Whereas the observer velocity creates a pure dipole anisotropy on the sky, the fluid velocity v_γ causes an rms spatial temperature variation $V_{\parallel} = \frac{1}{\sqrt{3}}v_\gamma/c$ on the last scattering surface from its line-of-sight component.⁶ For a photon-dominated $m_{\text{eff}} \simeq 1$ fluid, the velocity contribution is equal in amplitude to the density effect¹⁵ $V_{\parallel} = \frac{1}{3}\Psi \sin(ks)$.

The addition of baryons changes the relative velocity contribution. As the effective mass increases, conservation of energy requires that the velocity decreases for the same initial temperature displacement. Thus the *relative* amplitude of the Doppler effect scales as $m_{\text{eff}}^{-1/2}$. In the toy model of a constant baryon-photon momentum ratio R , the contribution becomes $V_{\parallel} = \frac{1}{3}\Psi(1 + 3R)(1 + R)^{-1/2} \sin(ks)$. Notice that velocity oscillations are symmetric around zero leading to an even more prominent compressional peaks (see Fig. 1a). Even in a universe with $\Omega_B h^2 \simeq 10^{-2}$ given by nucleosynthesis, R is sufficiently large to make velocity contributions subdominant.

Driving Effect

All realistic models involve time-dependent potentials. Forced acoustic oscillations result and can greatly enhance the peaks if the forcing frequency matches the natural frequency. Such is the case if the acoustic perturbations themselves generate most of the force through their self-gravity.^{16,17}

We have hitherto assumed that matter dominates the energy density. In reality, radiation dominates above the redshift of equality $z_{\text{eq}} = 2.4 \times 10^4 \Omega_0 h^2$, assuming the usual three flavors of massless neutrinos. We show in Box 1 how radiation fluctuations introduce a distinct class of *isocurvature* perturbations and distinguishes them from adiabatic ones by the associated driving mechanism. In both cases, the driving effect boosts the amplitude of the oscillations and leaves an imprint of the matter-radiation transition in the CMB. The critical scale corresponds to the wavenumber crossing the horizon at z_{eq} , $k_{\text{eq}} = 7.3 \times 10^{-2} \Omega_0 h^2 \text{ Mpc}^{-1}$. For adiabatic fluctuations, acoustic oscillations smaller than this scale are boosted by a factor of ~ 5 above the Sachs-Wolfe plateau in temperature. The peak-to-plateau ratio thus probes k_{eq} and so $\Omega_0 h^2$.

Photon Diffusion

In reality, coupling is imperfect since the photons possess a mean free path to Compton scattering λ_C . As the photons random walk through the baryons, hot and cold regions are mixed. Fluctuations damp nearly exponentially as the diffusion length $\lambda_D \sim \sqrt{N} \lambda_C = \sqrt{c \eta \lambda_C}$ overtakes the wavelength.⁸

At last scattering, the ionization fraction x_e decreases due to recombination, thus increasing the mean free path of the photons $\lambda_C \propto (x_e n_b)^{-1}$. The effective diffusion scale k_D can therefore be used as a probe of the ionization history and the baryon content $\Omega_B h^2$. Notice that this scale is not dependent on the nature of the initial fluctuations assumed (*cf.* Box 1). If recombination is delayed, *e.g.* by the early release of energy from particle decays or non-linear fluctuations, diffusion continues. As the diffusion length reaches the sound horizon, the acoustic peaks vanish. This occurs in models where recombination never occurred. We will return, below, to consider the less extreme variant of recombination followed by late reionization.

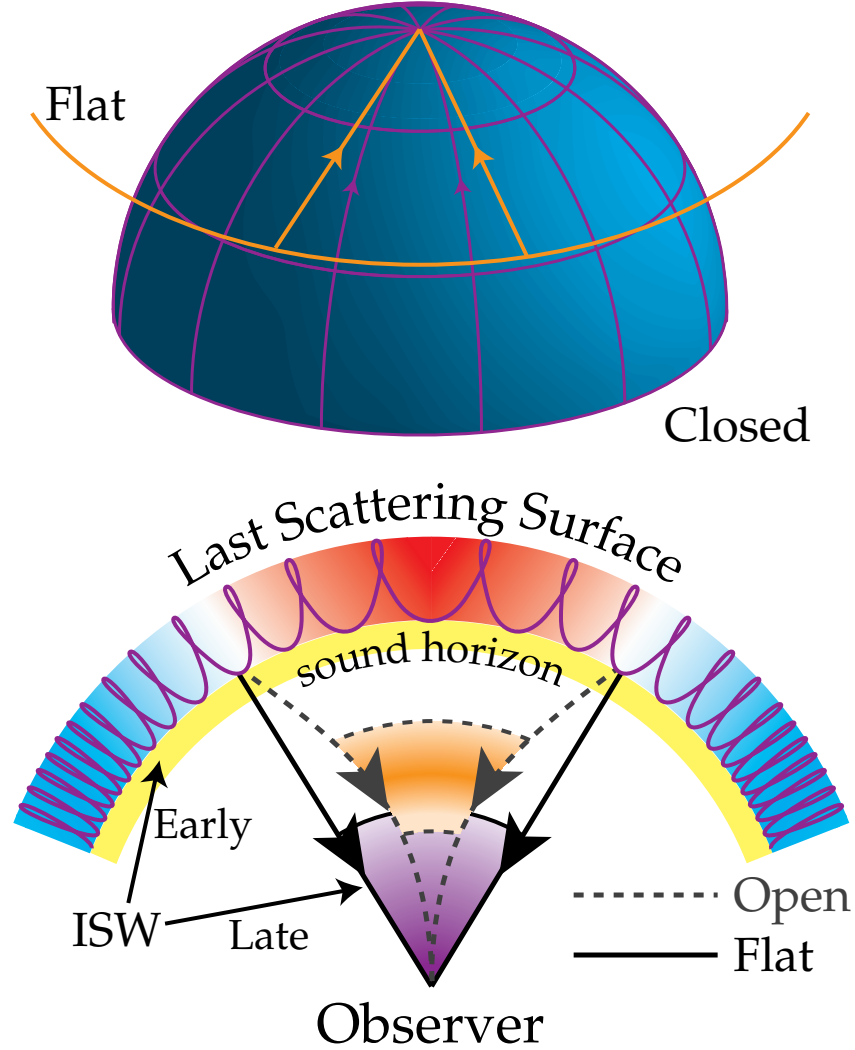


Figure 2. Projection effects. Temperature fluctuations on a distant surface appear as anisotropies on the sky. The angular size depends on the geometry of the universe and the distance to this surface. At a fixed distance, a smaller physical scale is required to subtend the same angle in a closed universe and larger in an open universe (schematically flattened for clarity). Acoustic fluctuations from last scattering subtend a smaller angle on the sky than the ISW effects for the same physical scale.

Projection Effect

The description of the primary signal now lacks only the relation between fluctuations at $z \simeq 10^3$ and anisotropies today. A spatial fluctuation on this distant surface appears as an anisotropy on the sky. Two quantities affect the projection: the curvature of the universe and the distance to the surface. The curvature is defined as $K = -H_0^2 \Omega_K / c^2$. Here the relative contribution of the curvature to the expansion rate is $\Omega_K = 1 - \Omega_0 - \Omega_\Lambda$, with Ω_Λ related to the cosmological constant as $\Lambda = 3H_0^2 \Omega_\Lambda / c^2$.

Consider first the case of positive curvature. Photons free stream to the observer on geodesics analogous to lines of longitude to the pole (see Fig. 2). Positive curvature (closed universe $K > 0$) makes the same

physical scale at fixed latitude (distance) subtend a larger angle than in the Euclidean case. The opposite effect occurs for negative curvature^{15,18} (open universe $K < 0$).

Increasing the distance to the last scattering surface also decreases the angular extent of the features. The distance to last scattering $c(\eta_0 - \eta_*)$ depends mainly on the expansion rate and hence on H_0, Ω_0, Ω_K and very weakly on Ω_Λ . Putting these quantities together gives us the angular diameter distance $d = |K|^{-1/2} \sinh[|K|^{1/2} c(\eta_0 - \eta_*)]$ for $K < 0$ and similarly for $K > 0$ with $\sinh \rightarrow \sin$. The angular extent $\theta \sim \ell^{-1}$ of a physical feature in the CMB is given by $\ell_{\text{feature}} = k_{\text{feature}} d$. These scales, especially the peak spacing ℓ_A based on k_A , provide angular size distance measures of the curvature.^{17,19} Combined, they allow one to reconstruct the other fundamental cosmological parameters through their effect on the various physical scales (*e.g.* k_A, k_{eq}, k_D) associated with the temperature fluctuations (see Box 2).

Secondary Anisotropies

Intervening effects between recombination and the present can alter the anisotropy. These divide basically into two categories: gravitational effects from metric distortions and rescattering effects from reionization. Both leave imprints of the more recent evolution of the universe and the structure within it. Compared with the primary signal, secondary anisotropies provide more details on the evolution of structure and less robust constraints on the background parameters.

Gravitational Effects

If metric fluctuations evolve as the photons stream past them, they leave their mark as gravitational redshifts.⁷ Common manifestations include, the early ISW effect from the radiation, the late ISW effect from rapid expansion, the Rees-Sciama effect from non-linear structures, and external sources such as gravitational waves and topological defects. Metric fluctuations can also lens the photons and distort the primary signal.

Consider first the gravitational redshift from ordinary scalar fluctuations. Here the metric fluctuations are the now familiar Newtonian potential Ψ for the time-time component and the curvature perturbation Φ for the space-space component. As we have already seen, gradients in the potential Ψ cause gravitational infall and redshift. If the depth of the potential well changes as the photon crosses it, the blueshift from falling in and the redshift from climbing out no longer cancel. This leads to a residual temperature fluctuation. To understand what distortions to the spatial metric through Φ do to the photons, recall that as the universe expands, the wavelength of the photon is also “stretched” through dilation effects. Similarly, the overdensities which create potential wells also stretch the space-time fabric and change the wavelengths of the photons (see Fig. 3). For example, as the potential decays, the contraction of the photon wavelength blueshifts the CMB to higher temperatures. Since $\Phi \simeq -\Psi$, it doubles the gravitational effect on the CMB. This heuristic explanation holds for more complicated cases such as vector and tensor metric fluctuations.

Dilation Effect

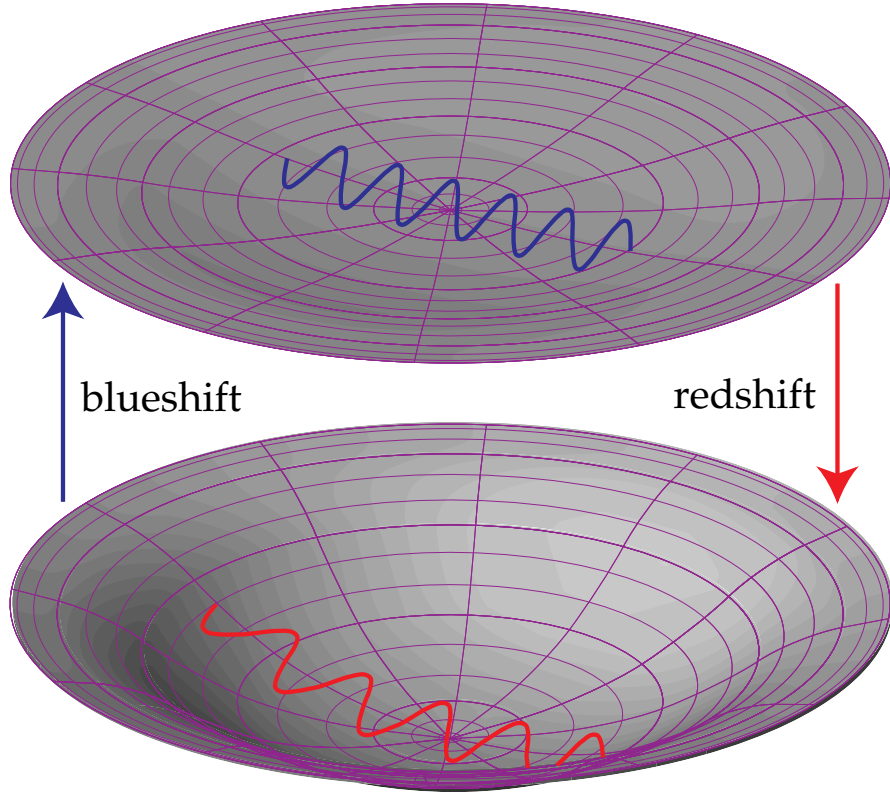


Figure 3. Dilation effect. Changes in the spatial metric distort the wavelength of passing photons. If the potential decays, the contracting curvature perturbation blueshifts the photons. If the potential grows, the corresponding “stretching” of space redshifts the photons. Since the curvature $\Phi \simeq -\Psi$, this effect doubles the ordinary potential redshift effect for both the driving force to the acoustic oscillator and the ISW effects.

Early ISW Effect. The early ISW effect arises if the universe is not completely matter dominated at last scattering.¹⁴ For adiabatic models, the potential decays for modes that cross the sound horizon between last scattering and full matter domination $k_{\text{eq}} \lesssim k \lesssim k_*$, yielding a net effect 5 times greater than the Sachs-Wolfe temperature plateau for $\Omega_0 h^2 \lesssim 0.04$. In isocurvature models, potential *growth* outside the sound horizon due to pressure fluctuations can contribute, which again is larger than the Sachs-Wolfe effect for $\Omega_0 h^2 \lesssim 0.04$. These effects are thus sensitive to $\Omega_0 h^2$ through the matter-radiation density ratio ρ_m/ρ_r . The one subtlety in this and the following effects is that it arises from a distance closer to the observer than the primary anisotropies so that the same physical scale subtends a larger angle on the sky (see Fig. 2).

Late ISW Effect. In an open or Λ model, the universe enters a rapid expansion phase once matter no longer dominates the expansion.²⁰ Matter-curvature equality occurs at $1 + z_K = \Omega_K/\Omega_0$ and matter- Λ equality at $1 + z_\Lambda = (\Omega_\Lambda/\Omega_0)^{1/3}$. Since the potential decays to zero within an expansion time, independent of the wavelength, it is the earlier of the two that matters $z_{K\Lambda} = \max[z_K, z_\Lambda]$. For the adiabatic case, the maximum is again 5 times greater than the Sachs-Wolfe temperature plateau. However opposing effects from decaying overdensities and underdensities tend to cancel if the photon can travel across many wavelengths during the decay. Thus, this effect is suppressed below the horizon at the decay epoch $k \gtrsim k_{K\Lambda}$. This scale is projected onto a multipole moment $\ell_{K\Lambda}$ in the same manner as the primary anisotropy. For a fixed Ω_0 , the decay epoch occurs much later in flat $\Omega_K = 0$ models than open $\Omega_\Lambda = 0$ ones. Thus Λ -models will suffer cancellation of late ISW contributions at a much larger scale than open models.¹⁶ Similar arguments hold for isocurvature models, save that the late ISW contribution exactly cancels the combined Sachs-Wolfe and early ISW effect for $\ell \ll \ell_{K\Lambda}$. In summary, a feature at $\ell_{K\Lambda}$ is expected in the CMB and can be used to constrain Ω_Λ in a flat universe or the curvature Ω_K of an open universe.²¹

Rees-Sciama Effect. Once fluctuations leave the linear regime, their subsequent evolution can also make the potentials vary with time.²² In hierarchical models, where the smallest scales go non-linear first, the effect peaks toward small scales. In most reasonable models, the non-linear scale is too small to significantly affect CMB observations above the arcminute regime.^{23,24} Although not likely to be observable by the next generation of experiments, the scale at which fluctuations become nonlinear ℓ_{NL} is in principle also imprinted on the CMB.

Tensors. Gravitational waves introduce tensor fluctuations in the metric. Rather than a pure temperature shift, these leave behind a quadrupole signature as they distort the distribution of passing photons.^{25,26} Gravitational waves redshift away inside the horizon so that their main effect on anisotropies occurs around horizon crossing. Thus only scales above the horizon at recombination $k \gtrsim k_*$ contribute significantly. The typical signature of gravity waves is an enhanced quadrupole $\ell = 2$ and a cut off at ℓ_* , the projected horizon at last scattering. If the same mechanism generates both the scalar and tensor fluctuations, there may exist a relation between their spectra. In particular, inflation predicts a consistency relation between the shape of the tensor spectrum and the tensor-to-scalar amplitude ratio which may provide a sensitive test of this paradigm.^{27,28}

Other External Sources. In general, any process that distorts the metric will produce corresponding distortions in the CMB. For example, topological defects may produce a spectrum of scalar, vector and tensor perturbations. Once generated, scalar and tensor perturbations affect the CMB as described above. Vector perturbations furthermore suffer decay from the expansion and are only important if continually generated by the source. Since their growth and decay is usually correlated with horizon crossing, equal amplitude metric fluctuations as a function of scale at this epoch produce a roughly scale-invariant spectrum of anisotropies (*cf.* Box 2).^{29,30}

Gravitational Lensing. Potential fluctuations also lens the CMB photons.^{31,32} Gravitational lensing smears out sharp features in the spectrum of primary anisotropy. In a scale-invariant adiabatic model with $\sim 10^{-5}$ potential fluctuations initially, the smearing is less than 10% in angle above 10 arcminutes.³³ This reflects the fact that lensing is a second order effect and should be a small perturbation to the temperature perturbation above the non-linearity scale.

Secondary Scattering.

Reionization can introduce an epoch during which the photons are recoupled to the electrons. Rescattering both erases primary anisotropies and generates new secondary ones. In models without large small-scale fluctuations initially, such as the scale-invariant adiabatic model, reionization sufficiently early to make the Compton optical depth $\tau \gtrsim 1$ is unlikely. We therefore implicitly assume that the following effects represent a perturbation on the primary signal.

Rescattering Damping. Rescattering damps fluctuations in the same manner as diffusion. Scattering eliminates anisotropies leaving them only in the unscattered fraction $e^{-\tau}$. Since outside the horizon, fluctuations are carried by isotropic temperature fluctuations, power is only lost on scales below the horizon at the rescattering epoch. Thus the damping envelope of Fig. B2 gains a dip at this scale which can in principle be used to measure or constrain the redshift of reionization.

Doppler Effect. Diffusion and rescattering prevents the appearance of large temperature fluctuations. However, the Doppler effect from scattering off electrons caught in the gravitational instability of the baryons can regenerate anisotropies.⁶ These contributions are also suppressed in the same way as the late ISW effect: photons that last scattered off overdensities and underdensities have Doppler shifts that tend to cancel.³⁴ If the underlying primary signal is known, the angular extent of the new fluctuations measures the horizon size at the rescattering epoch and their amplitude probes the baryon velocity at that time.

Non-Linear Effects. At very small scales, higher order contributions are more efficient than the Doppler effect in regenerating anisotropies. These generally make use of combining the Doppler effect with variations in the optical depth. Possibilities include linear perturbations in the baryon density (the Vishniac effect^{35,36}), inhomogeneities in the ionization fraction,³⁷ or contributions from clusters (the kinematic Sunyaev-Zel'dovich effect³⁸). Clusters can also produce anisotropic spectral distortions due to the upscattering of photons in frequency by hot electrons (thermal Sunyaev-Zel'dovich effect³⁸). In models without high amplitude small-scale power, it is unlikely that non-linear effects will dominate the total anisotropy in the observable regime.

Discussion

Primary anisotropy formation is a simple, well-understood linear process. The CMB anisotropy spectrum thus provides some of the cleanest and most robust cosmological tests available. Extraction of cosmological parameters from the primary fluctuations requires a specific model, but the number of unverified underlying assumptions is greatly reduced as the resolution reaches the several arcminute range. For example, the spacing between the peaks is a relatively robust probe of space curvature. It is determined from the sound horizon by the angular size-comoving distance relation and provides what is potentially the most sensitive and direct way to measure the geometry of the universe (see Fig. 4).

Obtaining other parameters will pose a greater challenge. In inflationary, *i.e.* near scale invariant adiabatic models, the morphology of the first peak is controlled by potential decay and baryon drag, which translate into additional dependences on $\Omega_0 h^2$ and $\Omega_B h^2$. The real advance will come with mapping of the higher peaks, where these various parameters have contrasting signatures on the peak heights and assumptions about the specific model may be relaxed.

To achieve these goals, coverage of a significant part of the sky is crucial. One needs a large number of independent patches at any specified angular scale to reduce the sampling variance. The ultimate or so-called

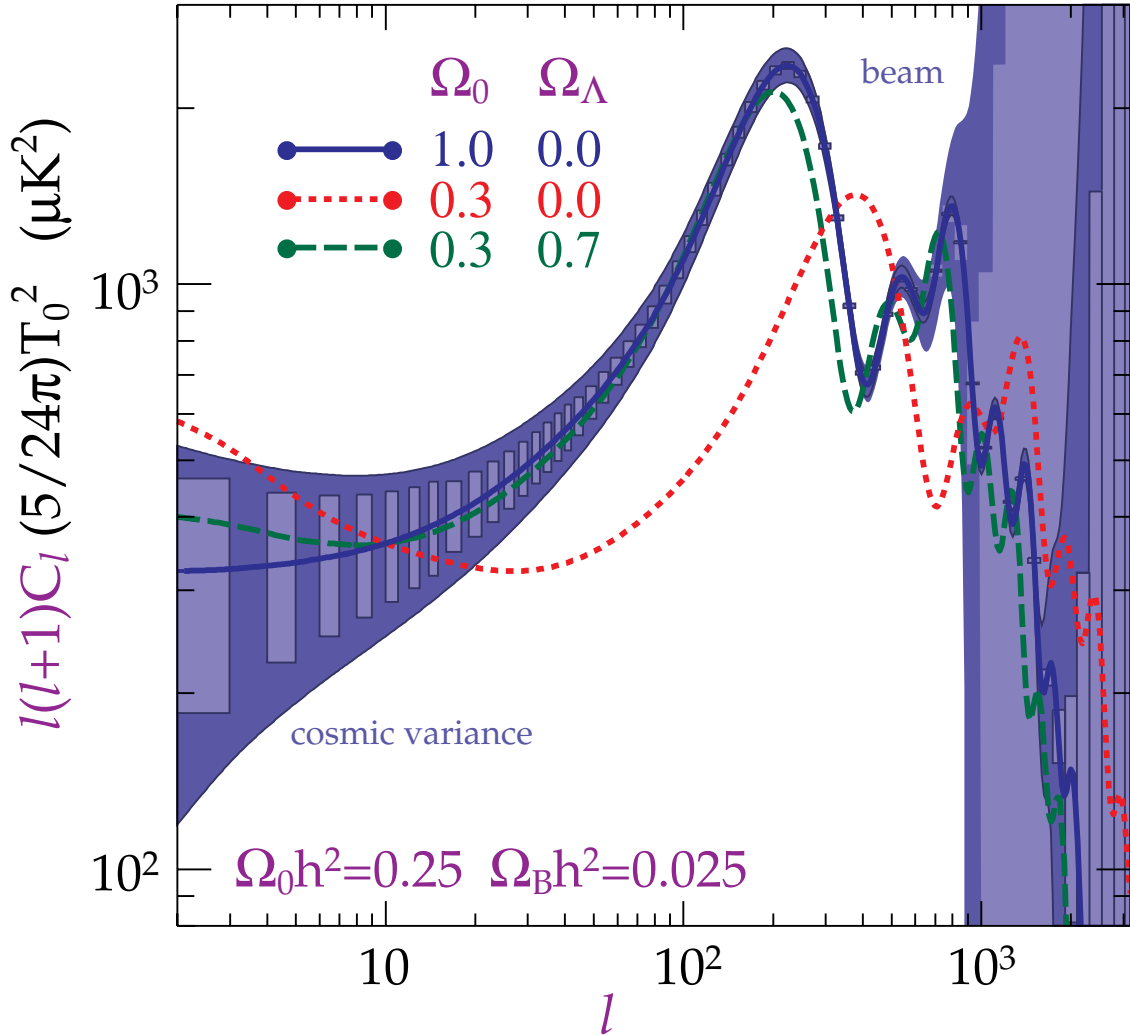


Figure 4. Idealized second ($20\mu\text{K}$ sensitivity on $18' \times 18'$ pixels) and third ($5.5\mu\text{K}$ on $10' \times 10'$ pixels) generation satellite experiments with full sky coverage. For an underlying inflationary model with $\Omega_0 = 1$, $\Omega_0 h^2 = 0.25$ and $\Omega_B h^2 = 0.025$ (dark blue curve), the power $\propto \ell(\ell+1)C_\ell$ at each multipole $\ell \propto \theta^{-1}$ can be recovered within the blue error contour (dark blue outline for the third generation). At low ℓ , deviations are due to “cosmic variance,” the same for both experiments; at high ℓ from the beam size and sensitivity. Binning better traces the smooth structure of the underlying power spectrum (light blue boxes $\simeq 10\%$ in ℓ). The $\Omega_0 = 0.3$ open and even the Λ variant (fixed $\Omega_0 h^2$ and $\Omega_B h^2$, normalized to $\ell = 10$) are easily distinguished under the inflationary paradigm. More robust parameter measurements require that several acoustic features be resolved by the third generation (*cf.* Box 2). In practice, foreground contamination will reduce the amount of sky available, increasing the errors as $f_{\text{sky}}^{-1/2}$, foreground subtraction will increase the noise, and secondary anisotropies will distort the spectrum at high ℓ .

“cosmic variance” limit is reached with a full sky map (see Fig. 4) although in practice some fraction of the sky will have to be discarded due to galactic foregrounds. Perhaps the greatest uncertainty lying ahead will be that of foregrounds due to unresolved sources. If at least half of the sky is mapped and relatively

foreground free, one should be able to measure most cosmological parameters presently being considered to a precision of better than a few percent with 10-20 arcminute resolution at a sensitivity currently attainable.

Acknowledgments

We would like to thank E. Bunn, D. Scott, and M. White for useful discussions. W.H was supported by the NSF and WM Keck Foundation.

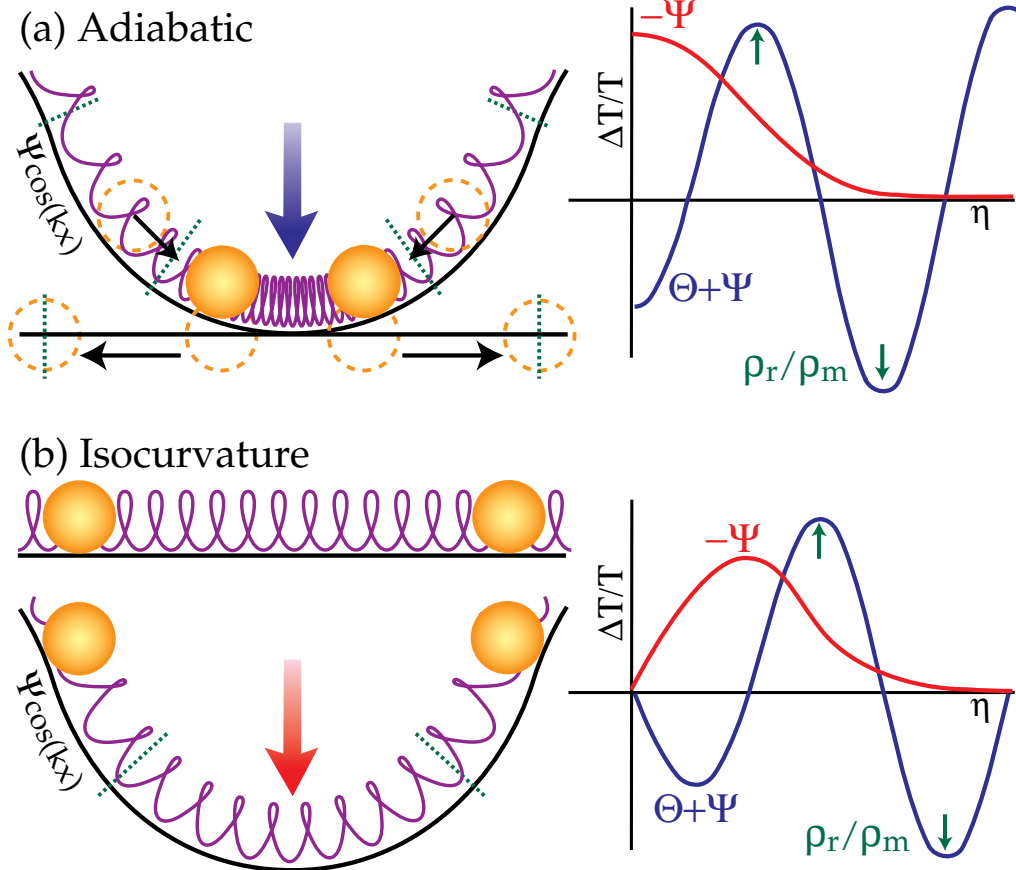


Figure B1. Driven oscillations. (a) Adiabatic case. As the fluid begins to compress, photon pressure resists the increase in the density perturbation thereby allowing the potential to decay. Left in a highly compressed state, the fluid then oscillates with enhanced amplitude. (b) Isocurvature case. Radiation fluctuations are set up to eliminate the potential initially. Photon pressure resists the accompanying rarefaction. The fluid then falls back into the well, lending its self-gravity to enhance the depth. At the compressional maxima, photon pressure again causes potential decay leaving the fluid in a highly compressed state. These feedback effects increase with the radiation-matter density ratio ρ_r/ρ_m driving a cosine oscillation in the adiabatic case and a sine oscillation in the isocurvature case.

Box 1: Adiabatic vs. Isocurvature Modes

Adiabatic and isocurvature models differ in their initial conditions. In the adiabatic case, number densities n of the different particle components fluctuate together. The resultant energy density perturbation δ generates a non-vanishing curvature fluctuation $\Phi = \frac{1}{2}\delta$ and a gravitational potential $\Psi \simeq -\Phi$. If radiation dominates, $\delta = \delta_r = 4\Theta$ whereas if matter dominates $\delta = \delta_m = \delta n_r/n_r = 3\Theta$. On the other hand, by balancing the initial fluctuations so that energy density perturbations cancel, isocurvature fluctuations may be established. Causality implies that the curvature perturbation remains constant until the matter can be redistributed.¹⁷ Thus in an isocurvature model, the gravitational perturbations only grow to be significant near horizon crossing. Since they represent the force felt by the oscillator, adiabatic and isocurvature conditions yield distinctly different acoustic signatures. The details of how the isocurvature fluctuation is set up, *e.g.* through

balancing radiation fluctuations with baryons, cold dark matter, or defects such as textures,³⁹ is not as important as the fact that potential fluctuations vanish initially and then grow in anticorrelation with the photon fluctuations until horizon crossing.¹⁷

In both cases, the self-gravity associated with the acoustic perturbation can feed back into the potentials to drive the oscillator. For the adiabatic mode, the initial potential perturbation is formed in large part by the photon-baryon density fluctuation. At horizon crossing, the photon-baryon fluid begins to compress itself due to its self-gravity and the effective temperature reverses sign. As pressure tries to stop the compression, the potential decays. The fluid is left in a highly compressed state. Thus self-gravity acts as a driving term timed to enhance the first compression of a $\cos(ks)$ series (see Fig. B1). This effect is doubled by dilation from the decaying curvature perturbation Φ (see Fig. 3). If self-gravity dominates, as in the case in which the universe was radiation dominated at horizon crossing, the fluid is left in a cosine oscillation with $2\Psi - \frac{1}{3}\Psi = \frac{5}{3}\Psi$ or 5 times the amplitude of the Sachs-Wolfe tail. Peaks occur at $mk_A = m\pi/s_*$ and baryon drag enhances all odd peaks.

In the isocurvature case, photon density fluctuations are initially balanced by those of the other species to eliminate the curvature. Photon pressure intercedes near horizon crossing to break this balance letting the potential fluctuation grow from zero. Still the photons attempt to compensate by becoming more and more underdense or rarefied inside potential wells $\Theta + \Psi \simeq 2\Psi < 0$ (see also Fig. 3). This continues until sound horizon crossing where photon pressure successfully resists further rarefaction (see Fig. B1). The fluid turns around and begins falling into the potential wells and furthermore enhances them by their self-gravity. As the photons resist further compression at the positive maximum, the self-gravity contribution to the potential fluctuation decays. This again leaves the photon-baryon fluid in a highly compressed state and increases the amplitude of the acoustic oscillation. Just as with the adiabatic case, the self-gravity of the photon-baryon fluid essentially *drives* the oscillator. Unlike the adiabatic case, it drives the sine rather than the cosine oscillation. Peaks occur at $k_m = (m - 1/2)k_A$ and baryon drag enhances all even peaks.¹⁶ The first peak, a result of superhorizon rarefaction required by photon compensation, is generally shallow and may be difficult to observe. Even so the harmonic series serves to distinguish the two cases through the ratio of peak location to separation $\ell_m/\ell_A = k_m/k_A$.

Isocurvature models can also possess exotic forcing mechanisms well inside the horizon which could overwhelm the signal described above. A rapidly varying potential can produce complicated acoustic spectra, and stochastic perturbations can entirely wash out peaks in the anisotropy spectrum.⁴⁰ However, gravitational potentials inside the horizon are difficult to generate and require extreme non-linear conditions.

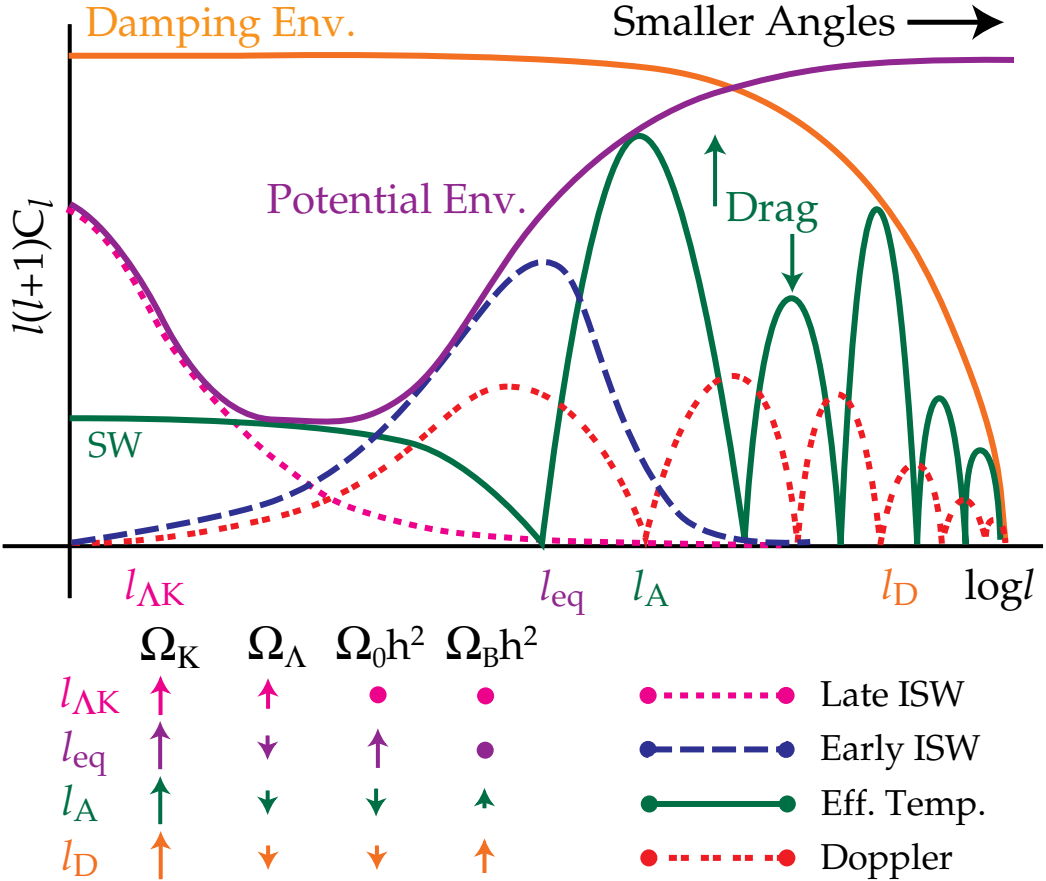


Figure B2. Anisotropy spectrum: power in anisotropies $\ell(\ell+1)C_\ell$ per logarithmic interval in $\ell \sim \theta^{-1}$. The decomposition into various physical effects allows one to extract four fundamental scales in the spectrum: $\ell_{\Lambda K}$ and ℓ_{eq} which enclose the Sachs-Wolfe (SW) plateau in the potential envelope, ℓ_A the acoustic spacing, and ℓ_D the characteristic scale of the diffusion damping envelope. Here a scale-invariant adiabatic case is shown for illustration purposes. These scales may be combined to infer the four fundamental cosmological parameters $\Omega_K (\equiv 1 - \Omega_\Lambda - \Omega_0)$, Ω_Λ , $\Omega_0 h$ and $\Omega_B h^2$. Baryon drag enhances all compressional (here odd) maxima of the acoustic oscillation, and can probe the spectrum of fluctuations at last scattering and/or $\Omega_B h^2$.

Box 2: Power Spectrum

The scale invariant adiabatic model illustrates how the anisotropy spectrum encodes cosmological information (see Fig. B2). It is conventionally denoted $\ell(\ell+1)C_\ell$ and represents the power per logarithmic interval in temperature fluctuations on angular scales $\ell \sim \theta^{-1}$. Highly accurate numerical results for the spectrum in this model have long been available^{41,42,43} with only moderate improvements to match the increasing precision of experiments^{44,45} (see also Fig. 4). Here we present a more schematic description that better illuminates the physical content and also may more easily be adapted to alternate models.

Several physical scales k_{feature} are imprinted in the angular power spectrum by the mechanisms described in the text. Furthermore, each known physical scale represents a standard ruler. This is converted to an angle on the sky as $\ell_{\text{feature}} = k_{\text{feature}}d$ by the angular diameter distance $d(K, \eta_0 - \eta_{\text{feature}})$.

The four angular scales imprinted on the CMB, $\ell_{K\Lambda}$, ℓ_{eq} , ℓ_A , and ℓ_D , form the fundamental basis for the spectrum. The first two scales appear because of the difference in potential evolution between the radiation, matter, and curvature- Λ dominated epochs. This defines a “potential envelope” as depicted in Fig. B2. The exact form of this envelope varies with the model but should generally bear the imprint of the two fundamental scales. For example, a baryon or axionic isocurvature model has an inverted form where the maximum contributions are between $\ell_{K\Lambda} \lesssim \ell \lesssim \ell_{\text{eq}}$ (see Box 1), and open adiabatic models may have less power at low ℓ due to a lack of super-curvature sized perturbations.^{49,50}

In the adiabatic case, the potential envelope also separates cleanly into three basic pieces: the late ISW fall, the Sachs-Wolfe (SW) plateau, and the early-ISW/driven oscillation rise. Driving effects produce temperature and sub-dominant velocity oscillations regularly spaced by ℓ_A . Photon diffusion provides a damping envelope with a characteristic scale ℓ_D that is entirely independent of the initial conditions (see Box 1).

For the standard thermal history and a universe composed of baryons, photons, cold dark matter, and neutrinos, these four scales can be combined to extract the four basic parameters^{16,46,47,48} Ω_K , Ω_Λ , $\Omega_0 h^2$, and $\Omega_B h^2$. Note that $\Omega_0 = 1 - \Omega_K - \Omega_\Lambda$ is not an independent parameter and hence the Hubble constant h may also be inferred from these measurements. We choose this representation since it is commonly supposed that either Ω_K or Ω_Λ vanishes and because the matter-radiation and baryon-photon density ratios control the physical processes in the early universe.

Since ℓ_A , the spacing between the acoustic peaks, is only weakly dependent on the other parameters and relies on the most distinctive features in the spectrum, it provides the cleanest measure of the curvature Ω_K . Even the degenerate but mild dependence on Ω_Λ can be removed by measurements or constraints on $\ell_{K\Lambda}$. The dramatic change in the potential envelope at ℓ_{eq} provides a sensitive probe of $\Omega_0 h^2$. In particular ℓ_{eq}/ℓ_A is entirely independent of Ω_K and Ω_Λ and only weakly dependent on $\Omega_B h^2$ thus serving to isolate $\Omega_0 h^2$. Even weaker effects such as the shift in ℓ_{eq} and ℓ_A from the neutrino mass and number are potentially observable^{45,51}. Unfortunately, a precise measurement of ℓ_{eq} must account for the damping envelope. Still, with complete information on the spectrum, no ambiguity arises. Baryon drag can also increase the height of the first peak but its signal in the higher peaks is unambiguous as it predicts alternating peak heights. The relative peak heights measure the baryon content times the potential at last scattering. To isolate Ψ_* , one can employ ℓ_A/ℓ_D which is independent of Ω_K and Ω_Λ and weakly dependent on $\Omega_0 h^2$ to measure the baryon content $\Omega_B h^2$. Aside from gross features set by the potential envelope, the relation between the peak locations and the peak spacing ℓ_m/ℓ_A , and Ψ_* from baryon drag, reveal the most valuable information about the model for the fluctuations that formed structure in the universe (see Box 1).

As discussed in the text, complications arise if other sources between recombination and the present are important. The damping envelope gains a step at the projected horizon of a late ionization epoch. New Doppler contributions can mask the damped peaks. Tensor modes can introduce features in the spectrum at $\ell < \ell_A$. Non-linear effects can alter the spectrum at $\ell > \ell_{\text{NL}}$. However, if these signals are subdominant, as is likely in many models, they will not destroy our power to measure fundamental cosmological parameters

from the gross features in the CMB. Furthermore they may allow a more detailed reconstruction of the thermal history and evolution of fluctuations since $z \sim 10^3$ using precision measurements.

References

1. Scott, D., Silk, J. & White, M. *Science* **268** 829-835 (1995)
2. Brandt, W.N. *et al.* *Astrophys. J.* **424** 1-21 (1994)
3. Tegmark, M. & Efstathiou, G. *Mon. Not. Roy. Astron. Soc.* (in press, astroph/9511148)
4. Smoot, G., *et al.* *Astrophys. J. Lett.* **396**, L1-L4 (1992)
5. Peebles, P.J.E. & Yu, J.T. *Astrophys. J.* **162**, 815-836 (1970)
6. Sunyaev, R.A. & Zel'dovich, Ya.B. *Astrophys. Space Sci.* **7**, 3-19 (1970)
7. Sachs, R.K. & Wolfe, A.M. *Astrophys. J.* **147**, 73-90 (1967)
8. Silk, J. *Astrophys. J.* **151**, 459-471 (1968)
9. Bardeen, J.M. *Phys. Rev. D.* **22**, 1882-1905 (1980)
10. Mukhanov, V.F., Feldman, H.A., & Brandenberger, R.H. *Phys. Rep.* **215**, 203-333 (1992)
11. Kaiser, N. & Silk, J. *Nature*, **324** 529-537 (1986)
12. White, M., Scott, D., & Silk, J. *Ann. Rev. Astron. Astroph.* **32**, 319-370 (1994)
13. Bond, J.R. *Theory and Observations of the Cosmic Microwave Background Radiation* (ed. Schaeffer, R.) (Elsevier, Netherlands, in press)
14. Hu, W. & Sugiyama, N. *Astrophys. J.* **444**, 489-506 (1995)
15. Doroshkevich, A.G., Zel'dovich, Ya.B., & Sunyaev, R.A. *Sov. Astron* **22**, 523-528 (1978)
16. Hu, W. & Sugiyama, N. *Phys. Rev. D.* **51**, 2599-2630 (1995)
17. Hu, W. & White, M. *Astrophys. J.* (in press astro-ph/9602019)
18. Sugiyama, N. & Gouda, N., *Prog. Theor. Phys.* **88**, 803-844 (1992)
19. Kamionkowski, M., Spergel, D.N., & Sugiyama, N. *Astrophys. J. Lett.* **434**, L1-L4 (1994)
20. Kofman, L.A. & Starobinskii, A.A. *Sov. Astron. Lett.* **9**, 643-651 (1985)
21. Sugiyama, N. & Silk, J. *Phys. Rev. Lett.* **73**, 509-513 (1994)
22. Rees, M.J. & Sciama, D.N. *Nature* **519**, 611-? (1968)
23. Seljak, U. *Astrophys. J.* **460**, 549-555 (1996)
24. Tuluie, R. & Laguna, P., *Astrophys. J. Lett.* **445**, L73-L76
25. Abbott, L.F. & Wise, M.B. *Nucl. Phys.* **B244**, 541-548 (1984)
26. Starobinskii, A.A., *Sov. Astron. Lett.* **11**, 113 (1985)
27. Davis, R. *et al.* *Phys. Rev. Lett.* **69**, 1856-1859 (1992); (erratum **70**, 1733)
28. Knox, L. & Turner, M.S., *Phys. Rev. Lett.* **73**, 3347-3350 (1994)
29. Coulson, D., Ferreira, P., Graham, P., & Turok, N. *Nature* **368**, 27-31 (1994)
30. Pen, U.L., Spergel, D.N., & Turok, N., *Phys. Rev. D.* **49**, 692-729 (1994)
31. Blanchard, A. & Schneider, J. *Astron. Astrophys.* **184**, 1-6 (1987)
32. Cole, S. & Efstathiou, G. *Mon. Not. Roy. Astron. Soc.* **239**, 195-200 (1989)
33. Seljak, U. *Astrophys. J.* **463** 1 (1996)
34. Kaiser, N. *Astrophys. J.* **282**, 374-381 (1984)
35. Ostriker, J.P. & Vishniac, E.T. *Astrophys. J. Lett.* **306**, L51-L58 (1986)
36. Vishniac, E.T. *Astrophys. J.* **322**, 597-604 (1987)
37. Aghanim, N., Desert, F.X., Puget, J.L., & Gispert, R. *Astron. & Astrophys.* (in press astro-ph/9604083)
38. Sunyaev, R.A. & Zel'dovich, Ya. B. *Comm. Astrophys. Space Phys.* **4**, 173-178 (1972)

39. Crittenden, R. & Turok, N. Phys. Rev. Lett. **75** 2642-2645 (1995)
40. Albrecht, A., Coulson, D., Ferreira, P. & Magueijo, J. Phys. Rev. Lett. **76** 1413-1416 (1996)
41. Wilson, M. & Silk, J. Astrophys. J. **243**, 14-25 (1981)
42. Bond, J.R. & Efstathiou, G. Astrophys. J. Lett **285**, L45-L48 (1984)
43. Vittorio, N. & Silk, J. Astrophys. J. Lett **285**, L39-L43 (1984)
44. Hu, W., Scott, D., Sugiyama, N. & Silk, J. Phys. Rev. D **52** 5498-5515
45. Ma, C-P. & Bertschinger, E. Astrophys. J. **455**, 7-25 (1995)
46. Bond, J.R. *et al.* Phys. Rev. Lett. **72**, 13-16 (1994)
47. Seljak, U. Astrophys. J. Lett. **435**, L87-L90 (1994)
48. Jungman, G., Kamionkowski, M., Kosowsky, A. & Spergel, astro-ph/9512139 (1995)
49. Bucher, M., Goldhaber, A.S., & Turok, N. Phys. Rev. D **52**, 3314-3337 (1995)
50. Yamamoto, K., Sasaki, M. & Tanaka, T. Astrophys. J. **455**, 412 (1995)
51. Dodelson, S., Gates, E. & Stebbins, A., astro-ph/9509147